Science of the Total Environment 743 (2020) 140828

Contents lists available at ScienceDirect

Science of the Total Environment

journal homepage: www.elsevier.com/locate/scitotenv

Galvanic oxidation processes (GOPs): An effective direct electron transfer approach for organic contaminant oxidation

Kuan Z. Huang, Huichun Zhang *

Department of Civil and Environmental Engineering, Case Western Reserve University, Cleveland, OH 44106, USA

HIGHLIGHTS

- The performance of GOP systems was evaluated under different solution conditions.
- IS showed a dual effect but the anions had little impact on BPA degradation.
- The electrodes had high stability and their hydration facilitated BPA degradation.
- Graphite itself without catalyst coating was also capable of shuttling electrons.
- The CSTR-GOP system achieved efficient and stable BPA degradation.

GRAPHICAL ABSTRACT

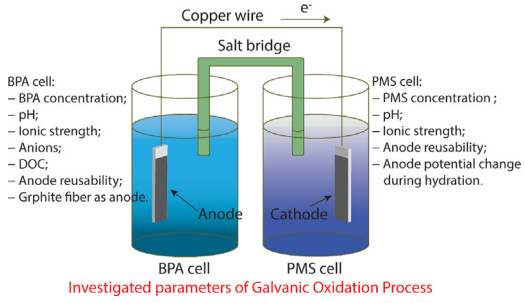

ARTICLE INFO

Article history:
Received 26 May 2020
Received in revised form 1 July 2020
Accepted 6 July 2020
Available online 8 July 2020

Editor: Jay Gan

Keywords:
Advanced oxidation processes
Direct electron transfer mechanism
Electrochemistry
Graphite electrode
Manganese oxide
Peroxymonosulfate

ABSTRACT

The activation of peroxymonosulfate (PMS) for organic contaminant oxidation usually relies on the formation of reactive oxygen species (ROSs). However, the ubiquitous anions and natural organic matter can easily scavenge ROSs and/or PMS, resulting in lower efficiencies and/or the formation of toxic byproducts. Relying on the unique long-distance electron transfer property, the recently developed Galvanic Oxidation Process (GOP) successfully achieved bisphenol A (BPA) degradation when BPA and PMS were physically separated in two reactors. In this study, we systematically investigated the performance of GOP at different PMS or BPA concentrations, pH, and ionic strength (IS) in both PMS and BPA solutions. The kinetic modeling employing the Langmuir-Hinshelwood model at different BPA concentrations suggested that although BPA and PMS were physically separated, the oxidation of the adsorbed BPA and reduction of the adsorbed PMS still followed a similar mechanism to that in traditional heterogeneous catalytic processes. The anions in the target water showed little impact on BPA degradation; higher IS enhanced the solution conductivity but inhibited BPA and electrode interactions, resulting in increased and then decrease BPA degradation rate. The electrodes presented high stability with a rate increase of 12% after 13 times of uses, and their hydration significantly facilitated BPA degradation but reduced the current by decreasing the potential difference between the anode and cathode. The graphite sheet itself without catalyst coating was also capable of shuttling electrons, while the use of a graphite fiber anode increased the BPA degradation by near 100% because of the larger surface area. The developed continuous stirred-tank reactor coupled with GOP (CSTR-GOP) achieved stable BPA degradation in less than 35 min and its scaling up is promising for future applications.

1. Introduction

Peroxymonosulfate (PMS)-based advanced oxidation processes (AOPs) are gaining growing attention in the oxidation of organic contaminants in water, mainly relying on the generation of radicals

* Corresponding author.
E-mail address: hjz13@case.edu (H. Zhang).

https://doi.org/10.1016/j.scitotenv.2020.140828
0048-9697/

including sulfate radicals ($SO_4^{\bullet -}$) and hydroxyl radicals (H•O). However, natural organic matter (NOM), halides including Cl^-, Br^-, and I^-, and other anions such as HCO_3^- and HPO_4^{2-} are ubiquitous in aquatic environments, and have been reported to be strong radical scavengers to significantly impact the removal efficiency of organic contaminants (Ghanbari and Moradi, 2017; Wang and Wang, 2018). Therefore, studies have developed a series of non-radical systems to overcome these issues by activating PMS for the formation of singlet oxygen ($^1O_2$) or through direct electron transfer pathways (Ahn et al., 2016, 2019; Huang and Zhang, 2019; Luo et al., 2019; Wang et al., 2018; Yun et al., 2018). However, PMS itself has been recognized to directly react with halides to form non-radical reactive halogen species such as HOCl, HOBr, and HOI, which can oxidize NOM and organic contaminants to form toxic halogenated byproducts, making the systems problematic (Fang et al., 2017; Ghanbari and Moradi, 2017; Huang and Zhang, 2020; Li et al., 2018; Wang and Wang, 2020). In addition, these systems suffer from drawbacks such as difficulty in catalyst recovery and secondary contamination due to chemical addition (Deng et al., 2018; Li et al., 2016; Peng et al., 2018; Ye et al., 2018). This has inspired us to develop a new treatment system that can overcome all the above issues.

Manganese oxides (MnOx) are attracting increasing attention for catalytic contaminant oxidation in AOPs because of their high reactivity, low toxicity, and large abundance in nature (Huang and Zhang, 2019). As doping can usually change the properties and improve the reactivity of a material, an iron (Fe^{3+})-doped manganese dioxide (δ-MnO_2) was prepared through the air oxidation of $MnSO_4$ solution under alkaline condition. Iron was selected as the dopant mainly because it is environmentally friendly, has similar physicochemical properties as manganese such as size, charge, and coordination tendencies, and can result in stable products. After a series of experiments, our recent study found that the obtained catalyst ($Fe_{0.15}Mn_{0.85}O_2$) can activate PMS to oxidize BPA through a direct electron transfer pathway (Huang and Zhang, 2019). By coating the catalyst onto two graphite electrodes that are connected by an external circuit and separating PMS and target water into two half cells, we have converted the traditional PMS-based AOP into a so-called Galvanic Oxidation Process (GOP) (Huang and Zhang, 2019). Relying on the excellent long-distance electron shuttling ability of the GOP, a common organic contaminant bisphenol A (BPA) was successfully degraded when PMS and BPA were physically separated. BPA was selected as the model compound mainly because it is widely present in the environment and its degradation has been extensively investigated in oxidation systems (Belfroid et al., 2002; Ma et al., 2019; Zeng et al., 2019). Another advantage of using nonradical-based catalysts is that the PMS decomposition only occurs when the catalyst and the substrate coexist, and the catalyst alone cannot cause the depletion of PMS (Ahn et al., 2016; Huang and Zhang, 2019; Wang et al., 2018; Zhang et al., 2014). This has made it possible for PMS not to be decomposed by the catalyst itself in GOP systems, which resulted in substantially higher PMS utilization efficiencies (the amount of substrate degraded per unit amount of PMS consumed) than in some of the traditional AOPs (Huang and Zhang, 2019).

Although GOP is an electrochemical method, it is substantially different from traditional electrochemical oxidations including Electrochemically Activated Persulfate (EAP) and Electrochemical Advanced Oxidation Processes (EAOPs). The EAP system usually consists of an external power supply and a pair of electrodes in the same working solution, in which radicals generated from the one-electron reduction of PDS/PMS at the cathode work as the major reactive oxygen species (ROSs) responsible for pollutant oxidation (Matzek and Carter, 2016; Matzek et al., 2018). A consumable anode may also be used to release metal ions into the working solution as the persulfate activator (Matzek and Carter, 2016). However, EAP systems generally require the addition of persulfates into the target water and both the system setup and reaction mechanisms are different from those of the GOP system. EAOPs are well-known for electrochemically generating oxidizing agents without chemical addition, including anodic oxidation and photoelectrocatalysis for the generation of heterogeneous H•O at the anode surface, and electro-Fenton, photoelectron-Fenton, and sonoelectrolysis for the generation of homogeneous H•O in bulk solution (Martinez-Huitle and Ferro, 2006; Sires et al., 2014). Reactive halogen species can be the major oxidizing agents in EAOPs when halides are present in the target water. Although some organic contaminants can be directly oxidized by the anode, a major portion of their removals is still due to the attack by the generated reactive agents. In addition, EAOPs require external power supplies or other types of energy inputs such as photo- and sonoirradiation. However, none of these are essential in GOPs. Therefore, no energy consumption is expected for this system.

Although the GOP was developed in our previous study, only a very basic concept was introduced and a deep understanding was not available. To obtain a better understanding of this system and evaluate the large-scale applicability, in this study, we systematically investigated the impact of operating conditions and water quality parameters on the removal of organic contaminants. BPA was selected as the probe compound because of its frequent presence in the environment (Belfroid et al., 2002). The iron-doped manganese oxide ($Fe_{0.15}Mn_{0.85}O_2$) was synthesized through air oxidation under alkaline conditions and was coated onto graphite sheet electrodes as the catalyst to enhance the electron transfer process. Because the PMS and BPA solutions were physically separated, we varied the water quality parameters of both the PMS and BPA solutions to investigate the BPA removal efficiency, including the PMS and BPA concentrations, pH, and ionic strength (IS). To better understand the reaction kinetics and the effect of BPA concentration, a kinetic model was developed based on the Langmuir-Hinshelwood (L-H) model to quantify the extent of BPA adsorption and relate it to the initial degradation rate. The L-H model has been extensively applied to investigate heterogeneous catalytic processes, such as PMS-based catalytic or TiO_2 photocatalytic degradation of organic contaminants, by assuming surface reaction as the rate-limiting step (Jadbabaei et al., 2017; Lowry and Reinhard, 2001; Wang et al., 2014; Xu et al., 2007; Zhu et al., 2005). To elucidate the matrix effects of water parameters on the GOP performance, we studied the BPA degradation in the presence of different anions and levels of dissolved organic carbon (DOC) that are common in surface water or hypersaline wastewater. The electrode stability was then tested for a total of 13 times of use, while the reactivities of the electrodes with and without the catalyst coating were compared. Furthermore, to simulate real-world applications, a continuous stirred-tank reactor (CSTR) was built with the GOP incorporated (i.e., CSTR-GOP) and its performance was examined.

2. Materials and methods

2.1. Chemicals

The chemicals used in this study were purchased from Fisher Scientific and Sigma Aldrich in reagent grade and used without further purification, including Oxone ($2KHSO_5 \cdot KHSO_4 \cdot K_2SO_4$, 98%), manganese chloride, sodium hydroxide, ferric chloride, sodium chloride, potassium chloride, sodium acetate, methanol, sodium perchlorate, sulfuric acid, acetic acid, potassium iodide, sodium bicarbonate, bisphenol A, and Leonardite humic acid.

2.2. Synthesis of the catalyst and preparation of electrodes

In this study, the iron-doped manganese oxide was synthesized through air oxidation and employed as the catalyst for preparing the electrodes. The synthesis details can be found in our previous study and the catalyst was characterized to be $Fe_{0.15}Mn_{0.85}O_2$ (Huang and Zhang, 2019). Briefly, $MnCl_2$ and $FeCl_3$ were dissolved in 50 mL deionized (DI) water at a molar ratio of 5:1. The solution was then aerated with air at a flow rate of 4 L/min and 80 mL NaOH solution was added dropwise into the mixture within a time period of 20 min. After 6 h of

reaction, the product was centrifuged and washed a few times with DI water and then transfer into KCl solution for ion exchange overnight. The product was washed thoroughly and dried at 65 °C overnight before a 2-h calcination at 200 °C. The catalyst was then ground into fine powder for later use.

To prepare catalyst suspension, 625 mg of the catalyst was added into 50 mL isopropanol together with 750 μL Nafion solution (15% in alcohol, Ion Power Inc.) as a polymer binder. The mixture was ultrasonicated for at least 1 h and agitated on a magnetic stirrer overnight to ensure even dispersion. To prepare the electrodes, graphite sheets (2.5 cm × 2.5 cm × 0.5 mm) were washed with DI water and dried at 65 °C for 1 h. Then, 100 μL of the suspension was added onto one side of a graphite sheet; after drying for 20 min, another 100 μL suspension was coated onto the same side. This process was repeated for the other side of the sheet and an evenly coated electrode was obtained.

2.3. Development of GOP and CSTR-GOP reactors

The salt bridge was built with 1.5% agar and NaCl or K_2SO_4, where K_2SO_4 was recommended to minimize the negative impact of the salt bridge on PMS decomposition as Cl^- can react with PMS. The mixture was heated at 200 °C under agitation until clear and then added into a U-shaped glass tube. After it was cooled down to room temperature, the salt bridge was applied to connect the two half cells to ensure electrical neutrality during the reaction. To minimize the effect of possible changes in the salt bridge during the reactions (e.g., electrolyte loss), each salt bridge was only used up to three times. Note that in real-world applications, a salt bridge can usually last much longer. The replacement of salt bridges is also easy and cheap to do because only salt needs to be replenished. Therefore, we believe this will not be a problem for real-world applications.

GOP systems were developed using the prepared electrodes and salt bridges with BPA and PMS present in two separate cells, as shown in Fig. 1 (dashed box). To study its performance on contaminant removal in a continuous flow, a CSTR coupled with GOP was developed with three identical graphite sheets in the BPA cell and one in the PMS cell (Fig. 1). Because the PMS had a concentration much higher than that of BPA (25 mM vs. 5 μM), the interactions between BPA and the anodes should be the rate-limiting step. Therefore, increasing the number of graphite sheets to three as anodes would be enough to maintain the BPA degradation at a high rate. The effluent was not returned to the water tank and the BPA concentration in the effluent was monitored.

2.4. Experimental procedure and analytical methods

For typical GOP reactions, BPA solutions of 5 μM were prepared in 50 mL beakers and buffered at pH 7 with 0.02 M borate buffer. 25 or 500 mM PMS solutions were prepared by dissolving Oxone powder into water. When 0.5 mM PMS was used, the working solution was obtained by diluting the 25 mM solution. Both BPA and PMS solutions were magnetically stirred at 250 rpm. To start the reaction, both electrodes were first immersed into the solutions to reach adsorption equilibrium unless otherwise specified. This process was completed in a short time, generally less than 25 min. This is also the prerequisite assumption for the L-H model that the adsorption reaches equilibrium very quickly and the surface reaction is the rate-limiting step. Then, the salt bridge was dipped in and the two electrodes were connected by a copper wire to initiate the reaction. The BPA concentration and the current between the two electrodes were monitored. For the CSTR-GOP system, the same BPA solution with a total volume of 1 L was pumped into a 50 mL reactor at a flow rate of 3.4 mL/min. The PMS solution was the same as that used in the GOP system. The BPA concentration in the effluent was then periodically monitored. The electrode reusability test was carried out for both electrodes for a total of 13 times of use in four days. The trials in each day were successively conducted without drying either electrode, whereas both electrodes were dried at room temperature in air overnight between each day.

To measure the potentials of the anode and cathode, a silver chloride reference electrode (Ag/AgCl) was employed with 1 M potassium chloride solution as the electrolyte. The measurement setup was similar to the GOP reactor (Fig. S1, Supplementary material), where the untargeted electrode was substituted by the reference electrode. By connecting the reference and the working electrode with a high impedance voltmeter, the potential difference was measured and the working electrode potential was expressed as "vs. Ag/AgCl" (Bard et al., 1980).

To analyze the BPA concentration, 1 mL sample aliquots were withdrawn at predetermined time intervals into 2 mL amber glass vials together with 30 μL hydroxylamine hydrochloride (1 M) to dissolve any possible catalyst that came into the solution. The residual BPA concentration was measured by a high-performance liquid chromatography (HPLC; Agilent 1260 Infinity II) equipped with a C18 column (Poroshell

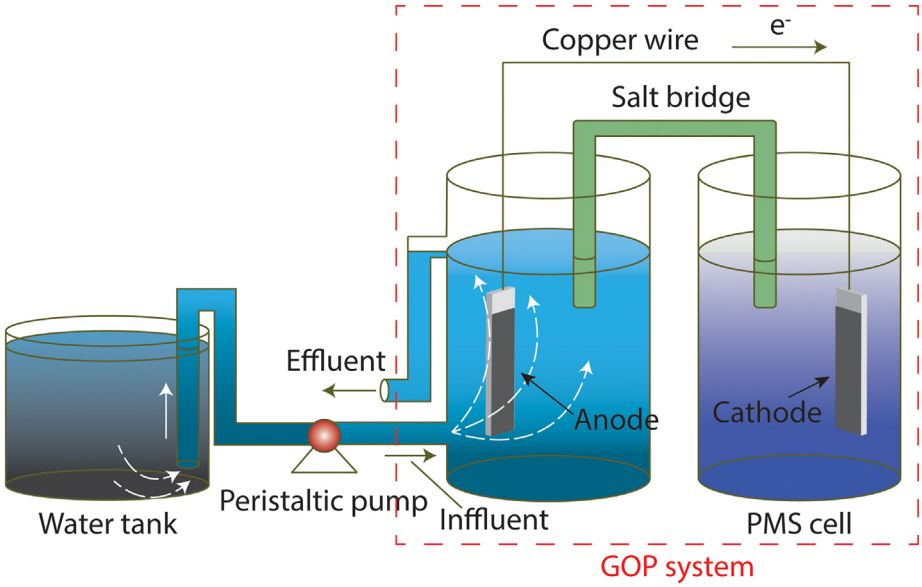

Fig. 1. A CSTR-GOP system for continuous water treatment.

120 EC-C18; 3.0 × 55 mm, 2.7 μm particle size) and a diode array detector. The mobile phase consisted of 0.1% acetic acid and methanol (v:v = 57:43) at a flow rate of 0.5 mL/min. The detection wavelength was set at 279 nm and the retention time was 2.898 min. The PMS concentration was determined based on its reaction with excess KI forming iodine, which was quantified at λ_{max} = 352 nm on a Cary Series UV–Vis spectrophotometer (Agilent) (Liang et al., 2008).

3. Results and discussion

3.1. Effects of PMS concentration, solution pH and IS in the PMS cell

Because PMS was present in a separate cell from the target water, it was easy to manipulate its conditions to optimize contaminant removal without disturbing the target water. In this study, three PMS concentrations of 0.5, 25, and 500 mM were investigated while the pH was controlled at 5 with 0.02 M acetate buffer. Due to the connection of the salt bridge, trace PMS might transport from the PMS cell to the BPA cell. However, this was not observed throughout the reaction (data not shown), suggesting that the BPA degradation was only attributed to the no-contact direct electron transfer. PMS was not decomposed by the electrode itself except for its ~4% adsorption in the first 20 min (Fig. S2), which was similar to the finding in the batch AOP system when no BPA was present (Huang and Zhang, 2019).

As shown in Fig. 2A, bare graphite sheets (electrodes without coating) did not result in any decrease in the BPA concentration when PMS was 0 mM as the adsorption had achieved equilibrium before sampling. However, the electrodes with coating led to a slight decrease in the BPA concentration. This might be due to the direct oxidation of BPA by the MnOx in the coating (Fig. 2A). As adsorption is generally considered to be much faster than the subsequent oxidation, the BPA oxidation during the adsorption period should be negligible (Jadbabaei et al., 2017). In contrast, once PMS was present, BPA degradation became much faster and the rate increased with increasing PMS concentration. For example, the pseudo-first order rate constant k increased from 0.004 to 0.014 and 0.023 min^{-1} with the increase in the PMS concentration from 0.5 to 25 and 500 mM, respectively. Because the BPA oxidation by the MnOx was much slower compared to that by PMS/MnOx, the k values represented the overall BPA depletion rates including the contributions of the oxidation by the catalyst. In addition, larger average currents between the two cells were observed, as shown in Fig. S3. This was reasonable because higher PMS concentrations can lead to higher conductivity and faster electron transfer and thus faster BPA oxidation.

It was reported that lower pH was beneficial for the complexation of PMS with the catalyst in the pH range of 5 to 13 (Huang and Zhang, 2019). In this study, we further explored the pH of 5, 2.3, and 1 (without buffering) because the PMS itself in the commercial name of Oxone was strongly acidic, with a pH of 2.3 at 25 mM. As shown in Fig. 2B, there was no significant difference in the k values at the three pH conditions, with a p value of 0.18 > 0.05 in an ANOVA test. This indicated that the interaction between PMS and the electrode was not further enhanced when the pH was below 5. δ-MnO_2 is reported to have a pH_{ZPC} (pH of zero point of charge) value of around 2.2–2.4 (Choi et al., 2014). The prepared catalyst was δ-MnO_2 doped with 1/5 iron (Fe^{3+}), but all our experimental results in both previous and current studies support that the pH_{ZPC} was near that value. Although the surface charge of the catalyst changed from negative to positive when pH decreased to below its pH_{ZPC}, the adsorption of negatively charged PMS (HSO_5^-, pKa = 9.4) did not increase significantly (Fig. S4). This agreed well with our previous work that the interaction between PMS and the catalyst was mostly inner-sphere complexation (Huang and Zhang, 2019). As the 25 mM PMS solution without buffering had a pH of 2.3, we adopted this condition for the rest of the tests.

In addition to the PMS concentration and pH, the effect of IS of the PMS solution was investigated. As shown in Fig. 2B, there was no significant change (p value of 0.39) in the BPA degradation rate with the addition of 50 and 500 mM $NaClO_4$ (total IS = 0.125 and 0.575, respectively), indicating that the IS negligibly impacted the interaction of PMS with the electrode and thus the oxidation of BPA. This is also in agreement with the finding that, similar to the surface charges, the solution IS did not affect the inner-sphere complexation between PMS and the catalyst (Zhang et al., 2019). For example, while working with inner-sphere complexation-based catalysts such as CuO, $CuFe_2O_4$ and α-Mn_2O_3@α-MnO_2, studies reported negligible effects of the IS on pollutant degradation in AOPs (Khan et al., 2018; Xu et al., 2016; Zhang et al., 2013; Zhang et al., 2019). For some other types of interactions such as outer-sphere complexation, however, the IS may pose a significant impact on the substrate degradation (Zhang et al., 2019).

3.2. Effect of BPA concentration and kinetic modeling

In addition to the conditions of the PMS solution, it is important to understand the impact of the water quality of the target water on contaminant removal. In this study, three BPA concentrations were first investigated. As shown in Fig. 3A, higher BPA concentrations resulted in smaller rate constants. The k values were found to be 0.012, 0.010, and

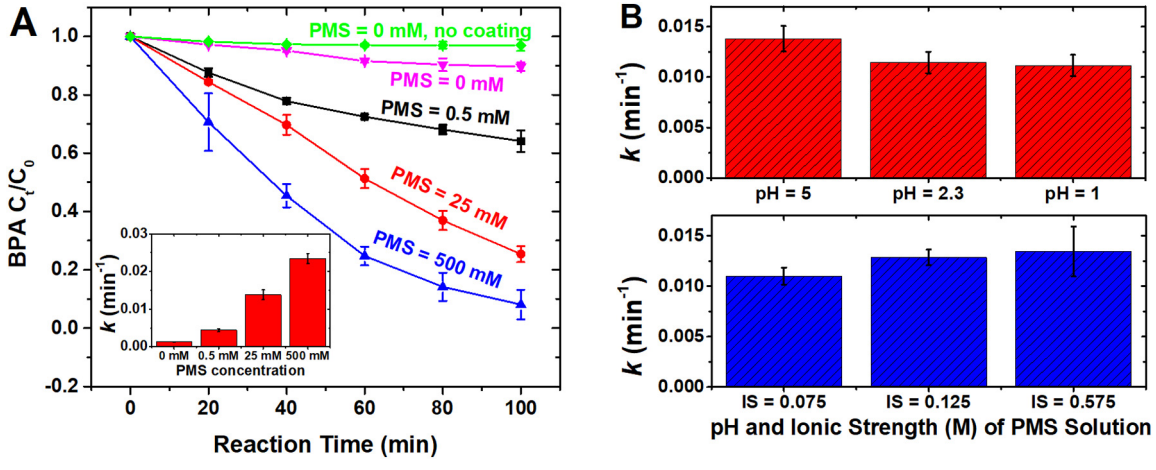

Fig. 2. (A) BPA degradation at different PMS concentrations. "PMS = 0 mM, no coating" means that the BPA concentration decrease was due to the adsorption by the pure graphite sheet, while "PMS = 0 mM" means that the BPA concentration decrease was due to the adsorption by the coated catalyst and graphite and the oxidation by the catalyst. (B) BPA degradation kinetics as quantified by the pseudo-first order rate constants k at different pH and IS conditions of the PMS solution. Other experimental conditions: $[BPA]_0$ = 5 μM; BPA pH = 7.0; $[PMS]_0$ = 25 mM for (B); Catalyst on each electrode = 50 mg. Error bars represent the data range of experimental replicates ($n \geq 2$).

0.005 min^{-1} when the BPA concentrations were 1, 5, and 50 μM, respectively. However, the degradation rates as well as the absolute amounts of BPA degraded per unit time were significantly larger at higher BPA concentrations. The larger amount of BPA adsorption from the bulk solution to the electrode surface (2.8, 11.6, and 26.8 μmol/g for the BPA concentrations of 1, 5, and 50 μM, respectively) might be the main reason. This also resulted in larger currents observed between the two electrodes (Fig. 3A). A kinetic model was then developed to better understand the reaction kinetics and the effect of BPA concentration based on the L-H model. By using the L-H model, for example, a study found that the substrate oxidation mainly happened at the surface of a catalyst by the attack of surface adsorbed radicals instead of in the bulk aqueous phase (Xu et al., 2016). In this study, according to the L-H model, the catalytic oxidation of BPA by the GOP system can be described in a few steps, including the rapid adsorption of both BPA and PMS onto the surface of the electrodes and then the reaction or electron transfer between the adsorbed species. The extent of BPA adsorption was quantified and related to the initial degradation rates. With the assumption that the surface reaction is the rate-determining step, the L-H model can be expressed as:

$$Step\ 1: BPA + * \overset{K_1}{\rightleftharpoons} BPA^{*} (\text{Adsorption of BPA}) \quad (1)$$

$$Step\ 2: PMS + * \overset{K_2}{\rightleftharpoons} PMS^{*} (\text{Adsorption of PMS}) \quad (2)$$

$$Step\ 3: BPA^{*} + PMS^{*} \overset{k_3}{\rightarrow} Product (\text{Surface reaction, rate-determining step}) \quad (3)$$

where * is the active adsorption site and BPA^{*}/PMS^{*} denotes the adsorbed BPA or PMS on the active adsorption site. K_1 and K_2 are the adsorption equilibrium constants while k_3 is the surface reaction rate constant. As BPA and PMS were physically separated in two cells, the adsorption of them was noncompetitive. At the beginning of the reaction, the adsorption of products was negligible due to their low concentrations. Therefore, the L-H model can be expressed as:

$$r_0 = k_r \frac{K_1[BPA]_0}{K_1[BPA]_0 + 1} \quad (4)$$

where r_0 is the initial reaction rate, $[BPA]_0$ is the initial BPA concentration, and k_r is the intrinsic rate constant ($k_r = k_3[PMS^{*}][*]_{0,\ BPA}$, where $[*]_{0,\ BPA}$ is the total adsorption site for BPA), often interpreted as the pseudo-first-order L-H-type rate coefficient on a monolayer surface (Xu et al., 2007). The derivation details of this model can be found in our previous study (Jadbabaei et al., 2017). Because the adsorption of BPA and PMS by the electrodes quickly reached maximum in less than 30 min while the surface reaction took up to 100 min, the surface reaction was believed to be the rate-determining step. Therefore, the r_0 should be similar to the BPA degradation rate monitored in the aqueous phase. To simplify the calculations, the r_0 used for modeling in this study was the initial aqueous phase BPA depletion rate, i.e., $k[BPA]_0$. With known values of r_0 and $[BPA]_0$ (Table S1), the L-H model showed a good fit against the experimental data with the fitted k_r and K_1 values of 0.448 mM/min and 0.025, as shown in Fig. 3B. The k_r value suggested that the system had an intrinsic rate constant of 0.448 mM/min. The small K_1 value indicated that the electrode had a low adsorption capacity for BPA, in agreement with the observed negligible BPA depletion due to adsorption alone. The good fitting to the L-H model is an indication that although BPA and PMS were physically separated in two cells, the oxidation of the adsorbed BPA still followed the same rule as in traditional heterogeneous catalytic processes.

3.3. Effect of solution pH and IS in the BPA cell

When studying the effect of pH, no significant difference was observed in BPA degradation at pH 5, 7, and 9 (Fig. 4A, p value = 0.75). This is in agreement with our previous study reporting that the adsorption was one of the main factors affecting substrate degradation. Since BPA has a pKa value of 9.9–11.3, most of the BPA species were in the neutral form in the pH range of 5 to 9 and their adsorption would not be affected significantly (Huang and Zhang, 2019). Therefore, the BPA degradation rate remained constant. The pH dependency should also apply broadly to other organic contaminants in that the pH effect is strongly dependent on their pKa values, which determines their adsorption.

Since different water matrices have different salinities, such as surface water, ground water, and hypersaline wastewater (Huang et al., 2018, 2019), the contaminant removal from those waters may depend on the IS. In this study, we examined an unbuffered solution and buffered solutions with 0.05, 0.5, or 2 M $NaClO_4$ (total IS ≈ 0, 0.013, 0.063, 0.513, and 2.013 M, respectively). As shown in Fig. 4B, the BPA degradation rate peaked at IS = 0.063 M with a rate constant of 0.014 min^{-1}, 186%, 24%, 18%, and 127% higher than that at IS ≈ 0, 0.013, 0.513, and 2.013 M, respectively. The increase of IS from 0 to 0.063 M would have led to higher solution conductivity resulting in faster electron transfer. Besides, the adsorption of BPA also increased with the increase of IS from 0 to 0.013 M (Fig. 4C, inset), which was beneficial for BPA oxidation. However, the further increase of IS from 0.013 to 0.513 M

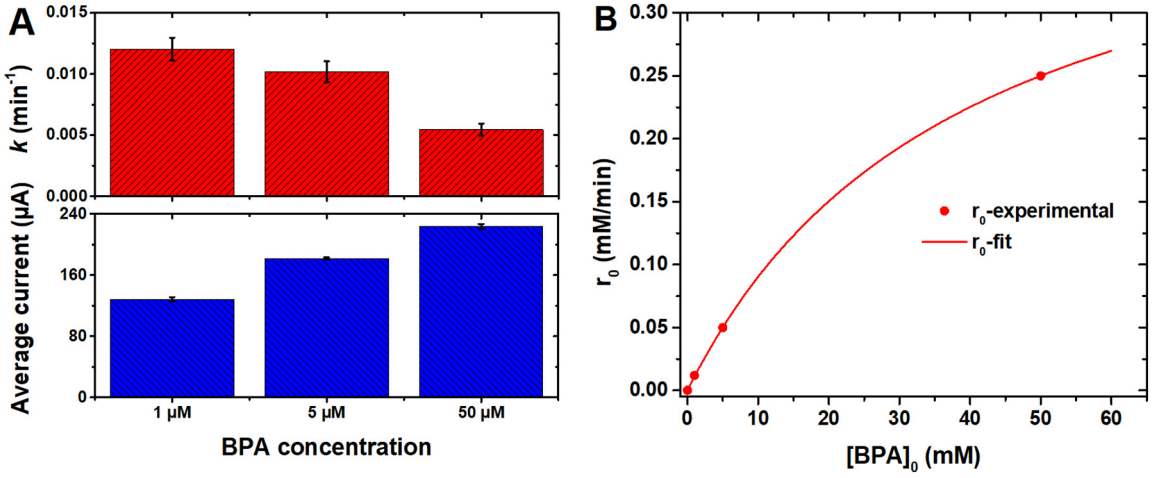

Fig. 3. (A) BPA degradation rate constants and average current at different BPA concentrations, and (B) kinetic modeling of the effect of initial BPA concentration on the initial BPA oxidation rate using the L-H model. Other experimental conditions: $[PMS]_0$ = 25 mM; PMS pH = 2.3; BPA pH = 7.0; Catalyst on each electrode = 50 mg. Error bars represent the data range of experimental replicates ($n \geq 2$).

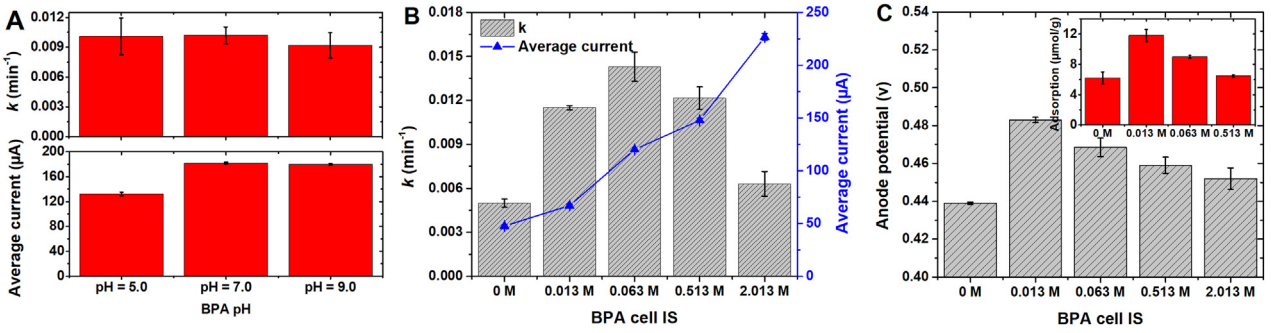

Fig. 4. BPA degradation rate constants and average current at different solution conditions including (A) pH and (B) IS in the BPA cell. (C) Anode potential and BPA adsorption at the catalyst surface at different IS. Other experimental conditions: $[PMS]_0 = 25$ mM; PMS pH = 2.3; $[BPA]_0 = 5$ μM; BPA pH = 7.0; Catalyst on each electrode = 50 mg. Error bars represent the data range of experimental replicates ($n \geq 2$).

suppressed BPA adsorption significantly (Fig. 4C, inset), exhibiting a "salting-in" effect. This effect happened when the excess cations competed with BPA to occupy the negatively charged catalyst surface through electrostatic attraction, resulting in less adsorption sites for BPA (Zhang et al., 2019). As a result, the BPA degradation was significantly inhibited. In addition, the anode potential is likely related to the BPA adsorption amount. As shown in Fig. 4C, the anode potential increased slightly and then decreased with increasing IS, which was in a similar trend to the change of BPA adsorption. However, it is yet unknown how the BPA adsorption affected the anode potential, which requires further investigation. The decrease in the anode potential and increased conductivity at higher IS could lead to an enhanced potential difference and therefore stronger current between the anode and cathode (Fig. 4B). It was reported that although the Na^+ and ClO_4^- did not participate in the electron transfer reaction, they can easily carry more than 90% of the current in the bulk solution because of their high concentrations (Bard et al., 1980).

3.4. Effects of anions and DOC

BPA degradation was also examined in the presence of different anions (5 mg/L NO_3^-, 40 mg/L HCO_3^-, 10 mg/L PO_4^{3-}, 40 mg/L SO_4^{2-}, or 10 mg/L Cl^-) (Tian et al., 2017) and DOC contents (0, 1, 5, 20, or 100 mg/L, prepared with humic acid) that are usually found in surface water. The IS changes due to the addition of these species were only between 8×10^{-5} and 1.3×10^{-3} M and their effect on BPA degradation was hence negligible. As demonstrated in Fig. 5A, most of the anions did not show significant impact on BPA degradation at the given concentrations (p value of 0.55). This suggests high stability of this treatment system toward different water matrices, which is substantially different from traditional PMS-based AOP systems, where most of the above species were reported to drastically lower the substrate removal efficiencies (Ghanbari and Moradi, 2017; Hu et al., 2018; Ma et al., 2018). The inhibition effect of PO_4^{3-} was more noticeable due to its strong complexation with the Mn in the catalyst (Schenk et al., 2005; Sharma et al., 2003; Yao and Millero, 1996; Zea et al., 2008), resulting in the suppressed activity of the catalyst (Zhang et al., 2013). This also led to the slightly lower current observed between the two electrodes. Except that, the currents in the presence of all other species were comparable. The major phosphate species is HPO_4^{2-} at pH 7 due to its second pKa value of 7.2. The reduction of HPO_4^{2-} to HPO_3^{2-} has a large negative redox potential of −690 mV (Schink and Friedrich, 2000), suggesting such a reduction reaction by capturing electrons from BPA is unlikely to occur. Therefore, the lower current in the presence of phosphate was primarily due to the lower BPA degradation rate.

DOC demonstrated an inhibitory effect on BPA degradation (Fig. 5B). This might be due to the attenuated adsorption of BPA at the electrode surface as a result of the competition of the humic acid for the adsorption sites (Fig. 5B) (Huang and Zhang, 2019). However, further inhibition on the BPA degradation was not observed when the DOC content was higher than 1 mg/L, suggesting that such an inhibitory effect was not proportional to the DOC level. When the DOC content was low, the inhibitory effect of DOC might be due to the quenching effect of the functional groups in the humic acid. However, if the electrode had limited sites for DOC, increasing the DOC content after all the sites have been occupied would not pose further inhibition on BPA degradation. On the other hand, studies have reported that humic acid is redox-active and can transfer electrons by serving as the electron shuttle under certain conditions (Aeschbacher et al., 2010; Klüpfel et al., 2014; Lovley et al., 1996). This process may compensate for the BPA

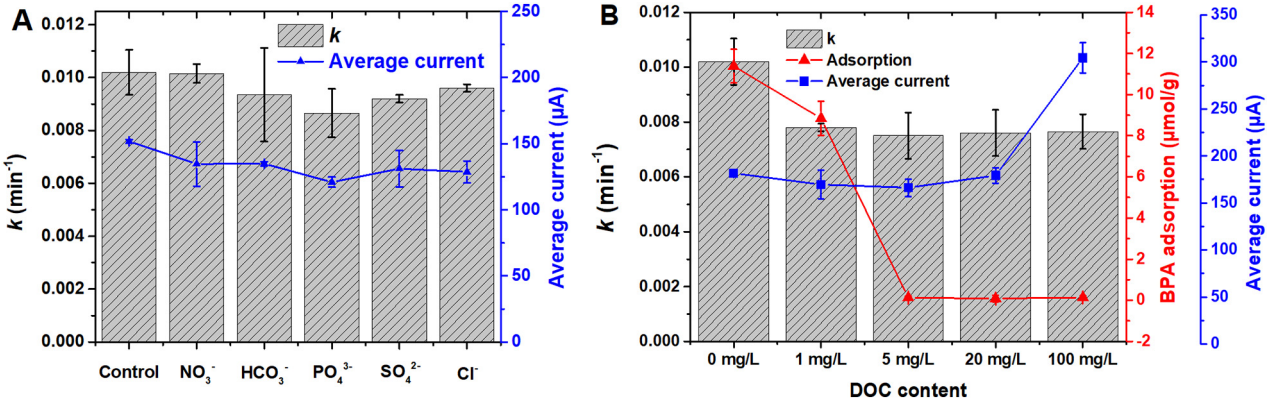

Fig. 5. BPA degradation in the presence of different (A) anions and (B) DOC contents. Experimental conditions: $[PMS]_0 = 25$ mM; PMS pH = 2.3; $[BPA]_0 = 5$ μM; BPA pH = 7.0; Catalyst on each electrode = 50 mg. Error bars represent the data range of experimental replicates ($n \geq 2$).

degradation at high DOC contents. This is significantly different from traditional radical- and nonradical-based systems, where the inhibitory effect usually becomes more pronounced as the DOC concentration increases (Gu et al., 2011; Ma et al., 2018; Wang et al., 2019). It has also been revealed that DOC can inhibit substrate oxidation much more significantly in radical-based systems than in nonradical ones (Ahn et al., 2016). The GOP system indeed demonstrated higher stability against DOC. The currents monitored between the two electrodes were comparable in the presence of 0–20 mg/L of DOC, but notably increased at 100 mg/L of DOC. This may indicate that some humic acid species were oxidized and contributed to the electron transfer which increased the current. Our previous study investigating the BPA degradation in both DI water and surface water also observed comparable PMS consumptions although the degradation rate in surface water was much lower than that in DI water (Huang and Zhang, 2019). This was a strong evidence of the oxidation of natural organic matter in the GOP system, although the extent of the DOC oxidation was much less than in radical-based systems.

3.5. Electrode reusability

The electrode reusability was examined for a total of 13 times of use. As illustrated in Fig. 6A, there was in general no significant decrease in the BPA degradation rate, suggesting high stability of the electrodes. By comparing the rates of the 1st and 13th uses, there was even a 12% increase due to the hydration of the electrodes. In addition, the BPA degradation rate continuously increased if both of the electrodes were reused without drying, while a decrease was observed once both of the electrodes were dried before use. This might be due to the different extent of hydration of the electrodes, which affected the interactions of the electrodes with BPA and PMS. As shown in Fig. 6B, soaking the anode in the BPA solution and the cathode in the PMS solution led to increase in the electrode potentials. However, the increase in the anode potential was much faster than that in the cathode, resulting in smaller potential differences. This might be the main reason that the current continuously decreased as the reaction continued (Fig. 6B). According to the Ohm's law $R = V/I$, the resistance of the system was found to be relatively stable during the hydration process. Similarly, the decrease in the current in the reusability test (Fig. 6A) might also be due to the smaller potential difference between the anode and cathode. In contrast, the dehydration during the overnight drying at room temperature reversed the process and led to lower BPA removal rates and increased currents. Therefore, in real-world applications, the use of new or regenerated electrodes at dehydrated conditions may result in strong currents upon the start of the system. Strategies such as presoaking may significantly improve the water treatment efficiency and reduce the current to help with the external circuit protection and safer operation.

3.6. Effect of catalyst coating on the electrode performance

To investigate the effect of the coated catalyst on the electron shuttling ability of the electrodes, we studied the BPA removal efficiency when neither, either, or both graphite sheets were coated with the catalyst. Different from our previous study observing that the graphite sheets alone did not show noticeable electron shuttling ability (Huang and Zhang, 2019), we did observe BPA degradation this time using pure graphite sheets as the electrode. This was likely because of the much higher PMS concentration employed in this study than that in the previous one (25 vs 0.5 mM), which led to much stronger interactions between PMS and graphite. Nevertheless, the coated electrodes still exhibited higher electron shuttling ability. As shown in Fig. 7A, compared to the bare graphite sheets, the coatings of either and both electrodes resulted in 30% and 55% faster BPA degradation, respectively.

To make the pure graphite electrode more applicable in the future, strategies should be taken such as using different shapes of graphite with higher surface areas such as shapes of fiber, foam, serpentine mesh, or forest to increase the reactivity (Fu et al., 2012; Logan et al., 2007; Luo et al., 2014). Furthermore, novel electrode materials in addition to graphite may be developed if they are capable of mediating electron transfer and have low manufacturing and regeneration costs.

To improve the efficiency of graphite itself, instead of using graphite sheets, we examined graphite in the form of fiber (UT-CF-3K, ACP) as the anode, as shown in Fig. 7B. The cathode was still the graphite sheet since the concentration of PMS (25 mM) was considerably higher than that of BPA (50 μM) such that the electron transfer between BPA and the anode was likely rate-limiting. As a result, the optimization of the electron transfer between BPA and the anode should be primarily considered. As shown in Fig. 7B (inset), after the adsorption had reached equilibrium at 70 min, the oxidation was initiated by dipping the salt bridge into the two cells and connecting the two electrodes by a copper wire. BPA was quickly degraded and completely removed in less than 300 min. The rate constant was calculated to be 0.01 min^{-1}, around 100% higher than that under similar conditions using the graphite sheet as the anode. Similarly, a previous study reported that the use of a graphite brush as the anode significantly enhanced the mass transfer and power production in a microbial fuel cell (Logan et al., 2007). This illustrates that the use of graphite anodes in different forms can

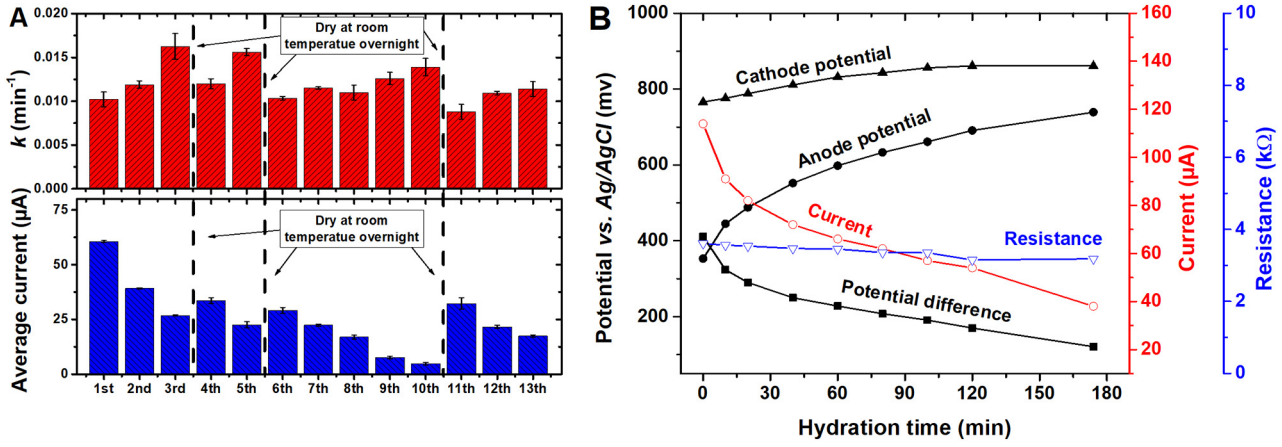

Fig. 6. (A) BPA degradation rate constants and average currents in a total of 13 times of use. (B) The change in electrode potential, potential difference, current and resistance during the soaking of the anode in the BPA cell and the cathode in the PMS cell. Experimental conditions: $[PMS]_0 = 25$ mM; PMS pH = 2.3; $[BPA]_0 = 5$ μM; BPA pH = 7.0; Catalyst on each electrode = 50 mg. Error bars represent the data range of experimental replicates ($n \geq 2$).

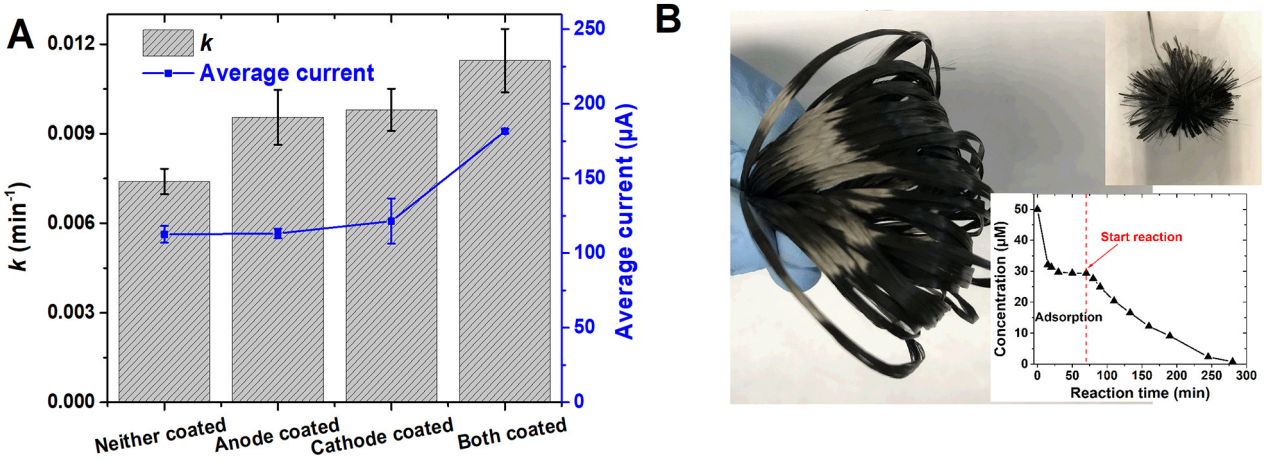

Fig. 7. (A) BPA degradation rate constants and average current change when neither, either, or both electrodes were coated with the catalyst, and (B) BPA adsorption and degradation kinetics using the graphite fiber anode. Experimental conditions: $[PMS]_0 = 25$ mM; PMS pH = 2.3; BPA pH = 7.0; $[BPA]_0 = 5$ μM for (A) and 50 μM for (B). Error bars represent the data range of experimental replicates ($n \geq 2$).

facilitate the reaction. The major advantages of using uncoated graphite as the electrode are that the electrode can be more easily prepared and be more easily and efficiently regenerated by approaches such as washing with organic solvents and baking under high temperatures without the concern of damaging the electrodes.

3.7. BPA degradation in a CSTR-GOP system

To simulate the applications in wastewater treatment, a CSTR was coupled with the GOP system as shown in Fig. 1. A total of 1 L water was pumped into the 50 mL reactor at a flow rate of 3.4 mL/min. The reactor was prefilled with 50 mL of BPA solution (part of the 1 L) before the reaction started. As shown in Fig. 8, the BPA concentration in the effluent rapidly decreased in the first 40 min and maintained at the steady state until the end of the test. Once the influent was cut off, the BPA concentration in the reactor quickly decreased. The PMS concentration was also measured during the process; due to its high concentration compared to BPA, its decrease was negligible. This also confirmed that PMS was stable in the cell in the presence of the electrode and any unwanted decomposition was negligible, suggesting that the PMS cell can act as an oxidant reservoir and be operated on a continuous basis.

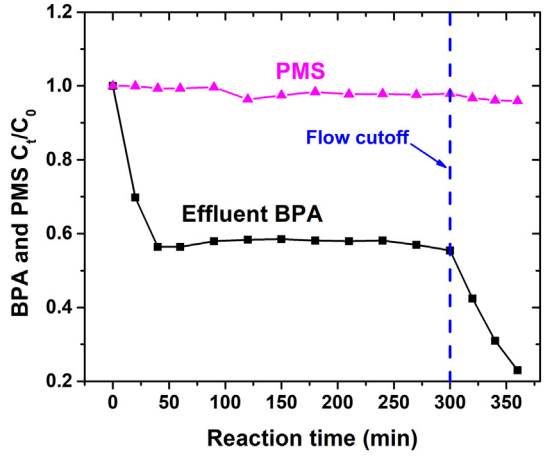

Fig. 8. The decrease in the BPA and PMS concentrations during the operation of a CSTR-GOP system. Experimental conditions: $[PMS]_0 = 25$ mM; PMS pH = 2.3; $[BPA]_0 = 5$ μM; BPA pH = 7.0; Three anodes and one cathode; Catalyst on each electrode = 50 mg; Total volume = 1 L; Flow rate = 3.4 mL/min.

3.8. Reaction mechanisms of the GOP system

The reaction in the PMS cell can be expressed as Eq. (5), where one PMS accepts two electrons from BPA to achieve PMS reduction and BPA oxidation. This is different from the commonly recognized one-electron PMS reduction to generate ROS, as shown in Eq. (6) (Yun et al., 2018). These two processes may occur simultaneously in some systems involving proper catalysts (Duan et al., 2018; Tang et al., 2018). In the GOP system, however, direct electron transfer should be the only process contributing to BPA degradation (Huang and Zhang, 2019).

$$HSO_5^- + 2e^- + H^+ \rightarrow SO_4^{2-} + H_2O \quad (5)$$

$$HSO_5^- + e^- \rightarrow SO_4^{\cdot -} + OH^- \quad (6)$$

In addition to PMS, other oxidants such as PDS and H_2O_2 could be used to accept electrons from contaminants. These oxidants could potentially replace PMS in GOP systems if they enable electron transfer as the major oxidation pathway, although future studies are needed to examine the detailed mechanisms.

Although some anions such as sulfate can be oxidized to produce radicals in some of the EAOPs especially when using anodes coated with diamond or PbO_2 (Sires et al., 2014), as shown in Eq. (7), this would not happen in GOP systems because these anions cannot participate in direct electron transfer reactions.

$$SO_4^{2-} \rightarrow SO_4^{\cdot -} + e^- \quad (7)$$

The redox couple $SO_4^{\bullet -}/SO_4^{2-}$ has a high reduction potential of 2.5–3.1 V_{NHE}, much higher than that of HSO_5^-/HSO_4^- at 1.4 V_{NHE} (Wacławek et al., 2017). Therefore, SO_4^{2-} is not likely to be oxidized by direct electron transfer. Our previous study on the batch system for BPA oxidation examined a series of approaches such as quenching methods, electron spin resonance analysis, and comparison with benchmark systems to identify the potential ROSs (Huang and Zhang, 2019). These system always contained at least 1 mM of SO_4^{2-} because Oxone (the triple salt $2KHSO_5 \cdot KHSO_4 \cdot K_2SO_4$) was used as the source of PMS. It would have been much easier for SO_4^{2-} to be oxidized in those batch reactors; however, no radicals were observed. In the GOP system, such reduction reaction would be even less likely. Similarly, other anion species such as phosphate and carbonate will not participate in the electron transfer reaction either.

Due to the selectivity of the GOP system, electron-rich compounds are expected to be more reactive. This has been a common

phenomenon for non-radical and direct electron transfer-based oxidation systems. Such selectivity can avoid competitive reactions with coexisting species such as natural organic matter in complex water matrices, which can otherwise significantly inhibit the degradation of target pollutants (Hu et al., 2017). Because of this property, the oxidation of BPA should start with losing electrons from the electron-rich moieties such as the hydroxyl and methyl groups resulting in the cleavage of the C—O and C—C bonds (Han et al., 2015; Li et al., 2008). BPA oxidation pathways and intermediates have been extensively reported in different electron transfer systems such as BPA oxidation by manganese oxides, ferrate, and persulfates (Han et al., 2015; Huang and Zhang, 2019; Li et al., 2008; Lin et al., 2009). Our recent study observed nine intermediates in the $Fe_{0.15}Mn_{0.85}O_2$/PMS/BPA system, such as 4-isopropenylphenol, p-isopropyl phenol, 2-phenyl isopropanol, and maleic acid (Huang and Zhang, 2019), some of which have also been found in other studies (Han et al., 2015; Lin et al., 2009). Although the toxicity may exhibit a hysteresis effect compared to the removal of BPA, it generally decreases quickly with the decrease of the BPA concentration (Han et al., 2015).

4. Conclusions

This study accomplished a systematic investigation of the impact factors on the oxidation of organic contaminants in a newly developed GOP system that does not require any chemical addition or catalyst dispersion into the target water. Different from most other studies on the use of PMS for water treatment, the GOP system does not rely on the generation of ROSs. Instead, the direct electron transfer between the two half cells is responsible for the contaminant degradation and PMS decomposition. Although the PMS concentration of 25 mM used in this system is much higher than those in traditional PMS-based batch AOPs (generally below 5 mM), those batch systems require the blending of PMS into the target water where a high PMS concentration can result in a significant waste of PMS and potential secondary contamination due to the PMS residual and produced SO_4^{2-}. However, this would not be a problem for GOP systems as PMS is stored in a separate container. No PMS waste or secondary contamination is expected. Compared to other electrochemical processes such as EAP or EAOPs, GOP also does not require an external power supply and no electrical energy consumption is needed.

Generally, higher PMS and BPA concentrations resulted in faster BPA degradation while the pH effect was highly dependent on the pKa values because the charged states of PMS and BPA determined their interactions with the electrode surfaces. The kinetic modeling employing the L-H model at different BPA concentrations suggested that although BPA and PMS were physically separated in two cells, the oxidation of the adsorbed BPA and reduction of the adsorbed PMS still followed a mechanism similar to that of traditional heterogeneous catalytic processes. The IS of the target water demonstrated a dual effect on the substrate degradation by enhancing the solution conductivity and inhibiting the substrate and electrode interactions. In addition, the GOP system showed high electrode stability and resistance toward a variety of anions and DOC in the target water. The bare graphite electrode without catalyst coating was also observed to shuttle electrons efficiently and its direct employment (especially in special shapes) can be considered for future applications. For a continuous water treatment system utilizing CSTR-GOP, the contaminant degradation was stable and its scaling up was promising for treating larger amounts of water with high contaminant removal efficiencies.

CRediT authorship contribution statement

Kuan Z. Huang: Conceptualization, Visualization, Data curation, Formal analysis, Writing - original draft. **Huichun Zhang:** Funding acquisition, Conceptualization, Visualization, Supervision, Writing - review & editing.

Declaration of competing interest

The authors declare that they have no known competing financial interests or personal relationships that could have appeared to influence the work reported in this paper.

Acknowledgements

This study was supported by the National Science Foundation Grants CBET-1762691 and CHE-1808406. We thank Dr. Jianzhi Huang for his help with the electrode potential measurement.

Appendix A. Supplementary data

Supplementary data to this article can be found online at https://doi.org/10.1016/j.scitotenv.2020.140828.

References

Aeschbacher, M., Sander, M., Schwarzenbach, R.P., 2010. Novel electrochemical approach to assess the redox properties of humic substances. Environ. Sci. Technol. 44 (1), 87–93.
Ahn, Y.Y., Yun, E.T., Seo, J.W., Lee, C., Kim, S.H., Kim, J.H., Lee, J., 2016. Activation of peroxymonosulfate by surface-loaded noble metal nanoparticles for oxidative degradation of organic compounds. Environ. Sci. Technol. 50 (18), 10187–10197.
Ahn, Y.Y., Bae, H., Kim, H.I., Kim, S.H., Kim, J.H., Lee, S.G., Lee, J., 2019. Surface-loaded metal nanoparticles for peroxymonosulfate activation: efficiency and mechanism reconnaissance. Appl. Catal. B-Environ. 241, 561–569.
Bard, A.J., Faulkner, L.R., Leddy, J., Zoski, C.G., 1980. Electrochemical Methods: Fundamentals and Applications. Wiley New York.
Belfroid, A., van Velzen, M., van der Horst, B., Vethaak, D., 2002. Occurrence of bisphenol A in surface water and uptake in fish: evaluation of field measurements. Chemosphere 49 (1), 97–103.
Choi, H., Woo, N.C., Jang, M., Cannon, F.S., Snyder, S.A., 2014. Magnesium oxide impregnated polyurethane to remove high levels of manganese cations from water. Sep. Purif. Technol. 136, 184–189.
Deng, J., Xu, M.Y., Qiu, C.G., Chen, Y., Ma, X.Y., Gao, N.Y., Li, X.Y., 2018. Magnetic $MnFe_2O_4$ activated peroxymonosulfate processes for degradation of bisphenol A: performance, mechanism and application feasibility. Appl. Surf. Sci. 459, 138–147.
Duan, X.G., Ao, Z.M., Zhang, H.Y., Saunders, M., Sun, H.Q., Shao, Z.P., Wang, S.B., 2018. Nanodiamonds in sp(2)/sp(3) configuration for radical to nonradical oxidation: Core-shell layer dependence. Appl. Catal. B-Environ. 222, 176–181.
Fang, C., Wang, Z., Feng, M., Huang, Y., Yang, F., Liu, J., 2017. Trace bromide ion impurity leads to formation of chlorobromoaromatic by-products in peroxymonosulfate-based oxidation of chlorophenols. Chemosphere 182, 624–629.
Fu, Y., Liu, J., Su, J., Zhao, Z., Liu, Y., Xu, Q., 2012. Electrochemical properties of electrodes with different shapes and diffusion kinetic analysis of microbial fuel cells on ocean floor. J. Ocean Univ. China 11 (1), 25–31.
Ghanbari, F., Moradi, M., 2017. Application of peroxymonosulfate and its activation methods for degradation of environmental organic pollutants: review. Chem. Eng. J. 310, 41–62.
Gu, X., Lu, S., Li, L., Qiu, Z., Sui, Q., Lin, K., Luo, Q., 2011. Oxidation of 1,1,1-trichloroethane stimulated by thermally activated persulfate. Ind. Eng. Chem. Res. 50 (19), 11029–11036.
Han, Q., Wang, H., Dong, W., Liu, T., Yin, Y., Fan, H., 2015. Degradation of bisphenol A by ferrate (VI) oxidation: kinetics, products and toxicity assessment. Chem. Eng. J. 262, 34–40.
Hu, P.D., Su, H.R., Chen, Z.Y., Yu, C.Y., Li, Q.L., Zhou, B.X., Alvarez, P.J.J., Long, M.C., 2017. Selective degradation of organic pollutants using an efficient metal-free catalyst derived from carbonized polypyrrole via peroxymonosulfate activation. Environ. Sci. Technol. 51 (19), 11288–11296.
Hu, L., Zhang, G., Liu, M., Wang, Q., Wang, P., 2018. Enhanced degradation of Bisphenol A (BPA) by peroxymonosulfate with Co_3O_4-Bi_2O_3 catalyst activation: effects of pH, inorganic anions, and water matrix. Chem. Eng. J. 338, 300–310.
Huang, K.Z., Zhang, H., 2019. Direct electron-transfer-based peroxymonosulfate activation by iron-doped manganese oxide (δ-MnO_2) and the development of Galvanic Oxidation Processes (GOPs). Environ. Sci. Technol. 53 (21), 12610–12620.
Huang, K.Z., Zhang, H., 2020. Highly efficient bromide removal from shale gas produced water by unactivated peroxymonosulfate for controlling disinfection byproduct formation in impacted water supplies. Environ. Sci. Technol. 54 (8), 5186–5196.
Huang, K.Z., Tang, H.L., Xie, Y.F., 2018. Impacts of shale gas production wastewater on disinfection byproduct formation: an investigation from a non-bromide perspective. Water Res. 144, 656–664.
Huang, K.Z., Xie, Y.F., Tang, H.L., 2019. Formation of disinfection by-products under influence of shale gas produced water. Sci. Total Environ. 647, 744–751.
Jadbabaei, N., Ye, T., Shuai, D., Zhang, H., 2017. Development of palladium-resin composites for catalytic hydrodechlorination of 4-chlorophenol. Appl. Catal. B-Environ. 205, 576–586.
Khan, A., Wang, H., Liu, Y., Jawad, A., Ifthikar, J., Liao, Z., Wang, T., Chen, Z., 2018. Highly efficient alpha-Mn_2O_3@alpha-MnO_2-500 nanocomposite for peroxymonosulfate

activation: comprehensive investigation of manganese oxides. J. Mater. Chem. A 6 (4), 1590–1600.
Klüpfel, L., Piepenbrock, A., Kappler, A., Sander, M., 2014. Humic substances as fully regenerable electron acceptors in recurrently anoxic environments. Nat. Geosci. 7 (3), 195–200.
Li, C., Li, X.Z., Graham, N., Gao, N.Y., 2008. The aqueous degradation of bisphenol A and steroid estrogens by ferrate. Water Res. 42 (1–2), 109–120.
Li, X., Wang, Z., Zhang, B., Rykov, A.I., Ahmed, M.A., Wang, J., 2016. $FexCo_3-xO_4$ nanocages derived from nanoscale metal–organic frameworks for removal of bisphenol A by activation of peroxymonosulfate. Appl. Catal. B-Environ. 181, 788–799.
Li, J., Zhou, Y., Jiang, J., Pang, S.-Y., Gao, Y., Yang, Y., Liu, G., Ma, J., Jiang, C., Wang, L., 2018. Transformation of phenolic compounds by peroxymonosulfate in the presence of iodide and formation of iodinated aromatic products. Chem. Eng. J. 335, 855–864.
Liang, C., Huang, C.F., Mohanty, N., Kurakalva, R.M., 2008. A rapid spectrophotometric determination of persulfate anion in ISCO. Chemosphere 73 (9), 1540–1543.
Lin, K., Liu, W., Gan, J., 2009. Oxidative removal of bisphenol A by manganese dioxide: efficacy, products, and pathways. Environ. Sci. Technol. 43 (10), 3860–3864.
Logan, B., Cheng, S., Watson, V., Estadt, G., 2007. Graphite fiber brush anodes for increased power production in air-cathode microbial fuel cells. Environ. Sci. Technol. 41 (9), 3341–3346.
Lovley, D.R., Coates, J.D., Blunt-Harris, E.L., Phillips, E.J.P., Woodward, J.C., 1996. Humic substances as electron acceptors for microbial respiration. Nature 382 (6590), 445–448.
Lowry, G.V., Reinhard, M., 2001. Pd-catalyzed TCE dechlorination in water: effect of $[H_2]$ (aq) and H_2-utilizing competitive solutes on the TCE dechlorination rate and product distribution. Environ. Sci. Technol. 35 (4), 696–702.
Luo, N., Ding, J., Zhao, N., Leung, B.H., Poon, C.C., 2014. Mobile Health: Design of Flexible and Stretchable Electrophysiological Sensors for Wearable Healthcare Systems. IEEE, pp. 87–91.
Luo, R., Li, M., Wang, C., Zhang, M., Nasir Khan, M.A., Sun, X., Shen, J., Han, W., Wang, L., Li, J., 2019. Singlet oxygen-dominated non-radical oxidation process for efficient degradation of bisphenol A under high salinity condition. Water Res. 148, 416–424.
Ma, J., Yang, Y., Jiang, X., Xie, Z., Li, X., Chen, C., Chen, H., 2018. Impacts of inorganic anions and natural organic matter on thermally activated persulfate oxidation of BTEX in water. Chemosphere 190, 296–306.
Ma, W.J., Wang, N., Du, Y.C., Tong, T.Z., Zhang, L.J., Lin, K.Y.A., Han, X.J., 2019. One-step synthesis of novel Fe_3C@nitrogen-doped carbon nanotubes/graphene nanosheets for catalytic degradation of bisphenol A in the presence of peroxymonosulfate. Chem. Eng. J. 356, 1022–1031.
Martinez-Huitle, C.A., Ferro, S., 2006. Electrochemical oxidation of organic pollutants for the wastewater treatment: direct and indirect processes. Chem. Soc. Rev. 35 (12), 1324–1340.
Matzek, L.W., Carter, K.E., 2016. Activated persulfate for organic chemical degradation: a review. Chemosphere 151, 178–188.
Matzek, L.W., Tipton, M.J., Farmer, A.T., Steen, A.D., Carter, K.E., 2018. Understanding electrochemically activated persulfate and its application to ciprofloxacin abatement. Environ. Sci. Technol. 52 (10), 5875–5883.
Peng, W., Liu, J., Li, C.X., Zong, F.X., Xu, W.S., Zhang, X., Fang, Z.D., 2018. A multipath peroxymonosulfate activation process over supported by magnetic CuO-Fe_3O_4 nanoparticles for efficient degradation of 4-chlorophenol. Korean J. Chem. Eng. 35 (8), 1662–1672.
Schenk, G., Gahan, L.R., Carrington, L.E., Mitić, N., Valizadeh, M., Hamilton, S.E., de Jersey, J., Guddat, L.W., 2005. Phosphate forms an unusual tripodal complex with the Fe–Mn center of sweet potato purple acid phosphatase. Proc. Natl. Acad. Sci. U. S. A. 102 (2), 273.
Schink, B., Friedrich, M., 2000. Phosphite oxidation by sulphate reduction. Nature 406 (6791), 37.
Sharma, C.V.K., Chusuei, C.C., Clérac, R., Möller, T., Dunbar, K.R., Clearfield, A., 2003. Magnetic property studies of manganese−phosphate complexes. Inorg. Chem. 42 (25), 8300–8308.
Sires, I., Brillas, E., Oturan, M.A., Rodrigo, M.A., Panizza, M., 2014. Electrochemical advanced oxidation processes: today and tomorrow. A review. Environ. Sci. Pollut. Res. Int. 21 (14), 8336–8367.
Tang, L., Liu, Y.I., Wang, J.J., Zeng, G.M., Deng, Y.C., Dong, H.R., Feng, H.P., Wang, J.J., Peng, B., 2018. Enhanced activation process of persulfate by mesoporous carbon for degradation of aqueous organic pollutants: Electron transfer mechanism. Appl. Catal. B-Environ. 231, 1–10.
Tian, X., Gao, P., Nie, Y., Yang, C., Zhou, Z., Li, Y., Wang, Y., 2017. A novel singlet oxygen involved peroxymonosulfate activation mechanism for degradation of ofloxacin and phenol in water. Chem. Commun. 53 (49), 6589–6592.
Wacławek, S., Lutze, H.V., Grübel, K., Padil, V.V.T., Černík, M., Dionysiou, D.D., 2017. Chemistry of persulfates in water and wastewater treatment: a review. Chem. Eng. J. 330, 44–62.
Wang, J., Wang, S., 2018. Activation of persulfate (PS) and peroxymonosulfate (PMS) and application for the degradation of emerging contaminants. Chem. Eng. J. 334, 1502–1517.
Wang, S., Wang, J., 2020. Treatment of membrane filtration concentrate of coking wastewater using PMS/chloridion oxidation process. Chem. Eng. J. 379, 122361.
Wang, Y., Liu, J., Wang, P., Werth, C.J., Strathmann, T.J., 2014. Palladium nanoparticles encapsulated in core–shell silica: a structured hydrogenation catalyst with enhanced activity for reduction of oxyanion water pollutants. ACS Catal. 4 (10), 3551–3559.
Wang, L., Jiang, J., Pang, S.Y., Zhou, Y., Li, J., Sun, S., Gao, Y., Jiang, C., 2018. Oxidation of bisphenol A by nonradical activation of peroxymonosulfate in the presence of amorphous manganese dioxide. Chem. Eng. J. 352, 1004–1013.
Wang, S., Xu, L., Wang, J., 2019. Nitrogen-doped graphene as peroxymonosulfate activator and electron transfer mediator for the enhanced degradation of sulfamethoxazole. Chem. Eng. J. 375, 122041.
Xu, T., Cai, Y., O'Shea, K.E., 2007. Adsorption and photocatalyzed oxidation of methylated arsenic species in TiO_2 suspensions. Environ. Sci. Technol. 41 (15), 5471–5477.
Xu, Y., Ai, J., Zhang, H., 2016. The mechanism of degradation of bisphenol A using the magnetically separable $CuFe_2O_4$/peroxymonosulfate heterogeneous oxidation process. J. Hazard. Mater. 309, 87–96.
Yao, W., Millero, F.J., 1996. Adsorption of phosphate on manganese dioxide in seawater. Environ. Sci. Technol. 30 (2), 536–541.
Ye, P., Wu, D., Wang, M., Wei, Y., Xu, A., Li, X., 2018. Coating magnetic $CuFe_2O_4$ nanoparticles with OMS-2 for enhanced degradation of organic pollutants via peroxymonosulfate activation. Appl. Surf. Sci. 428, 131–139.
Yun, E.T., Lee, J.H., Kim, J., Park, H.D., Lee, J., 2018. Identifying the nonradical mechanism in the peroxymonosulfate activation process: singlet oxygenation versus mediated electron transfer. Environ. Sci. Technol. 52 (12), 7032–7042.
Zea, C.J., Camci-Unal, G., Pohl, N.L., 2008. Thermodynamics of binding of divalent magnesium and manganese to uridine phosphates: implications for diabetes-related hypomagnesaemia and carbohydrate biocatalysis. Chem. Cent. J. 2 (1), 15.
Zeng, Y., Guo, N., Xu, X., Yu, Y., Wang, Q., Wang, N., Han, X., Yu, H., 2019. Degradation of bisphenol a using peroxymonosulfate activated by WO_3@MoS_2/Ag hollow nanotubes photocatalyst. Chemosphere 227, 589–597.
Zhang, T., Zhu, H., Croue, J.P., 2013. Production of sulfate radical from peroxymonosulfate induced by a magnetically separable $CuFe_2O_4$ spinel in water: efficiency, stability, and mechanism. Environ. Sci. Technol. 47 (6), 2784–2791.
Zhang, T., Chen, Y., Wang, Y., Le Roux, J., Yang, Y., Croue, J.P., 2014. Efficient peroxydisulfate activation process not relying on sulfate radical generation for water pollutant degradation. Environ. Sci. Technol. 48 (10), 5868–5875.
Zhang, Y., Zhu, C., Liu, F., Yuan, Y., Wu, H., Li, A., 2019. Effects of ionic strength on removal of toxic pollutants from aqueous media with multifarious adsorbents: a review. Sci. Total Environ. 646, 265–279.
Zhu, X., Castleberry, S.R., Nanny, M.A., Butler, E.C., 2005. Effects of pH and catalyst concentration on photocatalytic oxidation of aqueous ammonia and nitrite in titanium dioxide suspensions. Environ. Sci. Technol. 39 (10), 3784–3791.